Fan Ji, Mikko Juntunen, Iiro Hietanen, and Simo Eränen. 2007. Advanced photodiode detector for medical CT imaging: Design and performance. In: Proceedings of the 2007 IEEE International Symposium on Industrial Electronics (ISIE 2007). Vigo, Spain. 4-7 June 2007, pages 2730-2735.

Advanced Photodiode Detector For Medical CT Imaging: Design and Performance

Fan Ji, Mikko Juntunen, Iiro Hietanen
Detection Technology, Inc.
Vantaa, Finland
Email: ji.fan@deetee.com, mikko.juntunen@deetee.com

Simo Eränen
Micro and Nanoelectronics
Technical Research Center of Finland (VTT)
Espoo, Finland
Email: simo.eranen@vtt.fi

***Abstract*—This paper presents an advanced photodiode detector design for medical imaging applications, especially computerized tomography. The detector is silicon based and integrates the through-wafer interconnection technology into conventional front illuminated photodiode. The number of photodiode elements in the detector can be extended in 2D without reducing the photodiode active area. The signal of each photodiode element can be directly read out from the backside of the detector. Moreover, detectors can be tiled together in 2D without any physical limitation. A test photodiode detector was designed and demonstrated with 3x3 photodiode matrix arrangement in this paper. Different parameters were measured and analyzed from the demonstrated chip and test structures. The results show that the detector inherits most of the performance advantages from the conventional front illuminated photodiode, and all the parameters can either meet or exceed the requirements of modern CT systems.**

I. INTRODUCTION

The principle of the X-ray Computed Tomography (CT) for medical imaging is that an X-ray source gives out a fan beam or a cone beam of X-rays with certain energy and intensity, and the attenuation of the X-ray beam having penetrated the patient is recorded by an arc of photodiode detector arrays on the opposite side of the patient. With the synchronized rotation of the X-ray source and detectors around the patient, 2D cross section image or 3D information of the desired object inside the patient can be reconstructed.

For efficient volume scanning, spiral CT has been developed, in which the patient is controlled to continuously moving during the scanning through the rotating gantry, which is the ring structure carrying X-ray source and the detector arrays sampling the signals at the certain frequency. In addition, multi-slice detectors have been introduced to increase the volume scanning speed and enhance the spatial resolution. For instance, to scan a dynamic organ like the heart, the shorter the scanning time, the less distortion into the images will be caused by the patient and organ movements during the scanning. In order to further increase the scanning speed of the multi-slice CT machines, more detector coverage in 2D is required. Moreover, the pitch of two slices is getting smaller and smaller to increase the quality of the image. Some exemplary detector geometries used in modern CT systems can be seen in Table I [1], where the slice of the detectors is defined as the physical number of the rows along the gantry circumference direction.

TABLE I
MODERN CT SYSTEM WITH MULTI-SLICE DETECTORS

Manufacture	Scanner	No. of element slices	Year
GE	VCT 64	64	2004
Philips	Brilliance 64	64	2005
Siemens	SOMATOM Sensation 64	40	2004
Toshiba	Aquilion 64	64	2004
Toshiba	Beta site	256	2006

The development trend of increasing the amount of slices in modern X-ray CT detector for medical imaging application is facing serious limitations with the conventional photodiode detectors. The signals are wired out by metal lines which consume the surface area between the active photodiode elements in the conventional photodiode detectors. Therefore, only a certain maximum amount of slices can be constructed without sacrificing too much of the detector active area. The need of wire bonding pads for all of the signals on the edge of the detector chip gives another practical limitation to increase the number the slices. Furthermore, due to the wire bonding connections from the detectors to the substrate, detectors can not be fully tiled in 2D side by side. In addition to these limitations, once the detector elements exceed certain amount slices, the performance of the detector starts to decrease by parasitic factors like coverage efficiency, cross talk, electrical noise, etc.

Back illuminated Photodiode (BIP) detector has been reported to overcome the limitations encountered by conventional detectors [2] [3], but it has some drawbacks in both fabrication and operation. In order to effectively collect the photo current, very thin wafers and chips (typically 100μm thickness) have to be handled in the processing and assembly. On the other hand, the photo current is collected by carrier diffusion from the BIP's working principle, which slows down the operational speed and increases the cross talk between the adjacent elements. By introducing slot structures [2], BIP detector can minimize the cross talk to some level, but it

1-4244-0755-9/07/$20.00 ©2007 IEEE

deteriorates the mechanical stability and the productivity as side effect.

In order to achieve fully tileable detector arrays for medical imaging application without decreasing the productivity and performance of the detector, an advanced structure is presented in this paper. It integrates the through-wafer interconnection (TWI) technology [4] into the conventional front illuminated photodiode (FIP) detector. With the incoming light on the front surface of the detector, each signal of the detector elements can be extracted directly from the back side of the detector through TWI, meanwhile, keeping most of the performance advantages from FIP.

II. Design And Fabrication

A test photodiode detector with the 3x3 photodiode elements and the corresponding amount of TWIs were designed and demonstrated in this paper. The geometry of each photodiode element is designed and optimized for the application in the medical CT imaging. The photodiode element has an active area about $1mm^2$ and the pitch of approximately 1.25mm. The TWI for each photodiode element is located outside the active area and has the dimension of ϕ50μm. Each TWI consists of the isolated side wall and the conductive filling plug. The length of the TWI is that of the final thickness of the detector. The distance between the photodiode active area and the TWI is about 100μm. The anode of each photodiode element is connected to the top end of the TWI by a metal line on the front side. The corresponding contact pad for the anode on the back side is located directly on top the other end of the TWI. The cathode contact of each photodiode element is connected to the silicon bulk from the back side as well. The size of the contact pads is about 160μmx160μm. The cross section of individual photodiode element can be seen in Fig. 1. The light impacts on the front surface of the photodiode, and the generated photo current is collected by the anode and thereafter extracted out through the TWI from the pad on the back side.

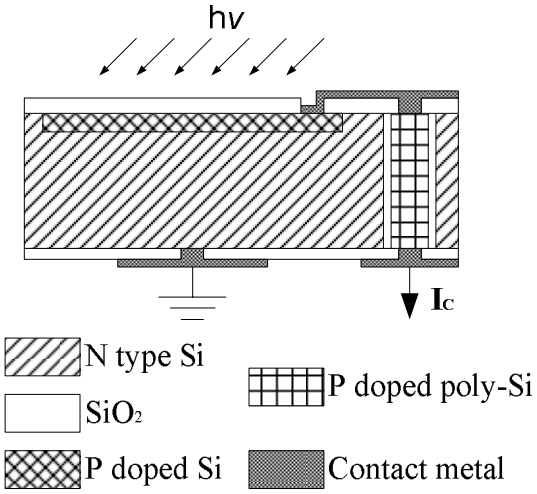

Fig. 1. Cross section of individual photodiode element structure

N type silicon wafer with suitable resistivity was selected as the substrate. The fabrication process started with the formation of TWIs. Inductively coupled plasma etching (ICP), thermal oxidation, in-situ doped polycrystalline silicon filling, grinding and chemical mechanical polishing (CMP) were used sequentially to fabricate the TWIs on the wafer. More details can be found in [4]. Since the structure and material of the interconnections are totally compatible with the standard silicon processing, photodiodes can be readily processed onto the pre-processed wafers already with TWIs. The p-type implantation was carried out to create active areas (anodes) on the front side, and the additional n-type implantation was carried to form better cathode contacts on the back side. Contact openings were etched out on the front side for both anode and TWI, and aluminum metallization was sputtered and patterned for the connection between the anode and the top end of the TWI. Contact openings were also etched on the back side for the cathode and TWI, followed by aluminum sputtering and patterning. Additionally, under bump metallization might be needed based on the selected packaging method. The simplified processing flow can be seen in Fig. 2. After the whole processing, the final detector thickness is about 300μm, which can be easily increased to 400μm.

The cross section of one processed photodiode with TWI can be seen in Fig. 3, where the PN junction area of the photodiode element was marked afterwards, because the implantation areas are not visible by the picture from microscopy. On the other hand, the TWI structure can be clearly seen. The serrated side wall close to the bottom is caused by the local etching in the ICP process. As long as it is protected by reasonable thickness of isolation, it will not affect the performance of the photodiode.

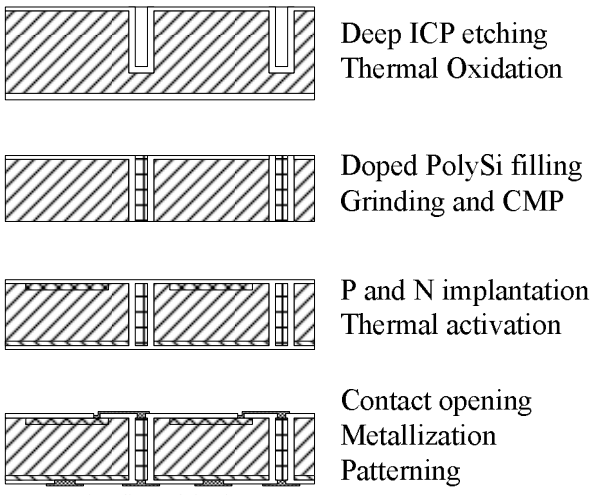

Fig. 2. Processing flow of the detector

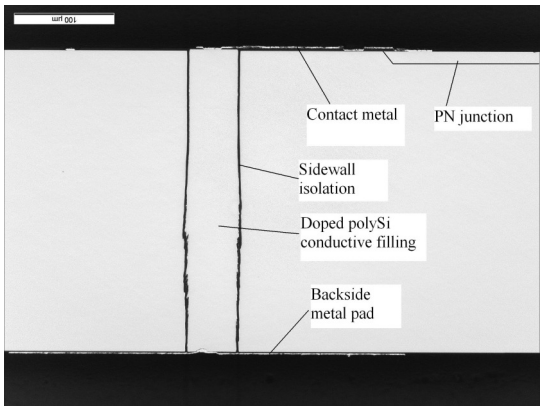

Fig. 3. Microscopy picture of the processed photodiode element structure

III. Methods And Results

A. Current versus voltage characteristics

Within a Karl SÜSS dark probe station, the current to voltage characteristics of all photodiode elements on the sample detectors were measured by using a HP semiconductor parameter analyzer. The current to voltage behaviors of nine photodiode elements on one sample chip can be seen in Fig. 4. The leakage current, series resistance, shunt resistance and breakdown voltage can be extracted from the measurement data.

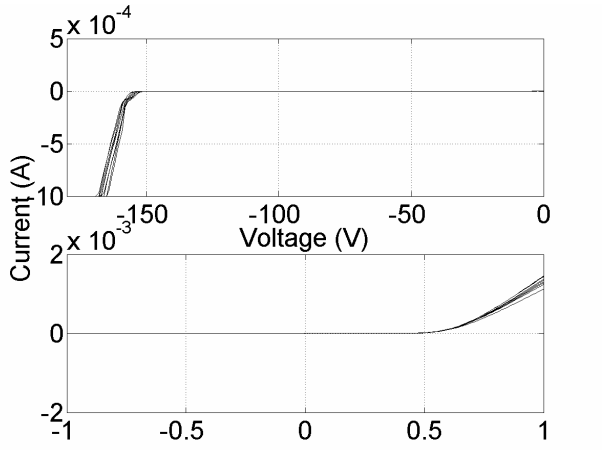

Fig. 4. The dark current of the photodiode elements under the bias voltage browsing from -180V to 1V at room temperature.

The leakage current is one of the important parameters for medical CT imaging, which partly influences the noise of the system. The average leakage current of the photodiode elements is about 0.5pA at the room temperature under 10mV reverse bias. The distribution of leakage currents of one tested chip is shown in Fig. 5. The sources of the leakage current in PN diode devices are well known mainly from the space charge region, bulk quasi natural region and surface interface region in terms of the saturation current, generation-recombination current and the surface current [5]. The design presented in this paper is such that the TWI is far enough outside the active area of the photodiode. Therefore, the TWI induced space charge region and surface interface are separated from photodiode active area by quasi natural regions and the isolation side wall. This results in the TWI having very small impact on the photodiode leakage current.

By commonly used definition of shunt resistance, the shunt resistance of the photodiode can be evaluated by the voltage current ratio under 10mV reverse bias. According to the leakage current data in Fig. 5, the average shunt resistance is about 20GΩ.

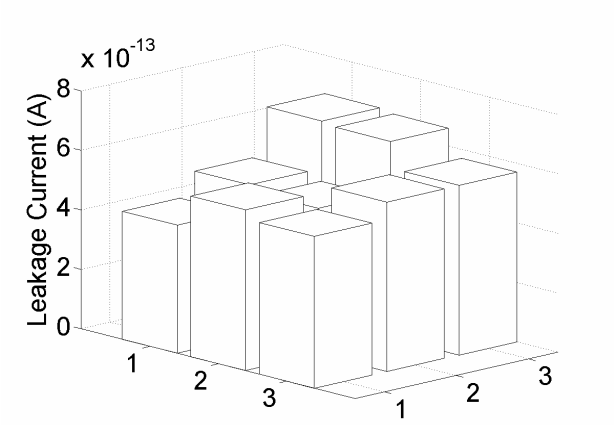

Fig. 5. The leakage current of individual photodiode element under 10mV reverse bias at room temperature.

The series resistance of the photodiode is another important parameter for CT system. The total resistance of a conventional photodiode element includes two contact resistances, silicon bulk resistance and the wire resistance. The length of a standard wire in conventional multi-slice FIP detector from center to the edge can be about 30mm with 6μm width, which gives 250Ω with aluminum sheet resistance of 50mΩ/□. This will cause a relatively large resistance difference between the center elements and edge elements of a conventional FIP detector. The uniformity of series resistances can be greatly improved by extracting signal through TWI besides each photodiode element. In the forward bias situation [6], considering the voltage falls on the series resistor, the series resistance of the photodiode can be deduced in the form of (1), where dV/dI is the dynamic series resistance measured under 1V forward bias, k is the Boltzmann's constant, T is the temperature in Kelvin, q is the electronic charge, I is the dynamic current under 1V forward bias and n_f is the ideality factor. The calculated series resistance value of the demonstrated photodiode detector in this paper is shown in Fig. 6 by assuming the ideality factor of 1.5. This gives about 230Ω on the average.

$$R_s = \frac{dV}{dI} - \frac{n_f kT}{qI} \quad (1)$$

The average breakdown voltage of each photodiode element is about 160V reverse bias, which can also be seen in Fig. 4. This is much higher than the requirement for the CT application. In addition, the breakdown voltage measured from individual TWI was over 200V reverse bias under the same measurement condition. Consequently, the TWI structure has no negative effect on photodiode breakdown characteristic.

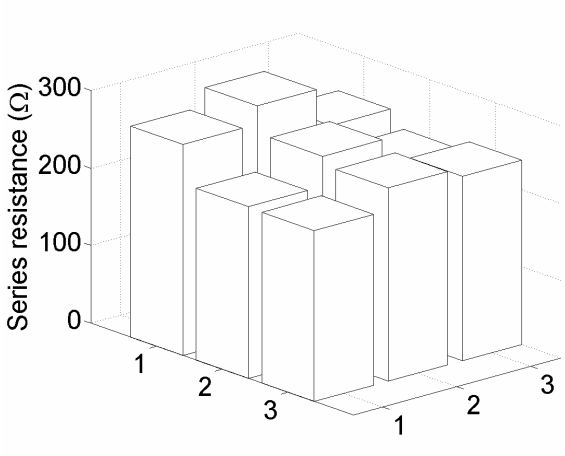

Fig. 6. The dynamic series resistance of individual photodiode element under 1V forward bias at room temperature.

B. *Capacitance versus voltage characteristic*

The capacitance of conventional FIP element consists of PN junction capacitance, line capacitance and bonding pad capacitance under normal working conditions of CT system. The metal lines induce not only parasitic capacitance to the silicon bulk, but also a small parasitic capacitance to each other. According to Schaper and Amey's model [7], the same metal line as discussed in the series resistance section can cause about 10pF parasitic capacitance, which proportionally increases the noise in the following preamplifier stage of the CT system. For the photodiode detector presented in this paper, the TWI capacitor replaces the wire capacitor in each photodiode element. The total capacitance of the photodiode elements with TWIs were measured by Keitheley CV analyzer and the results are shown in Fig. 7, where the dotted line presents the measured capacitance, and the "o" line is the calculated capacitance from the PN junction and contact pad with proper material parameters and dimension values. The capacitance of the pad capacitor can be calculated by using parallel plate model. The capacitance of a quasi PIN junction introduced by depletion region can be calculated by (2) according to [6], where A_j is the junction area, ε_s is the silicon permittivity, ϕ_i is the junction build-in potential, V is the bias voltage, N_d is the doping density in quasi intrinsic N type region, W indicates the width of the depletion region and W_i indicates the width of the quasi intrinsic region. The calculated capacitance might have bigger error under low reverse bias voltage, because one side abrupt junction is assumed instead of the real variation of the doping concentration in the quasi intrinsic region. But the calculated capacitance is more accurate under high reverse bias voltage because the extended depletion width can be neglected once the depletion width reaches the edge of the quasi intrinsic region. Therefore, the difference between two curves at high bias voltage point gives more precisely about the capacitance of the TWI, which is about 0.1pF under 5V reverse bias. It is fairly small when comparing to the pad and the junction capacitance.

$$\begin{cases} C_j = A_j\sqrt{\dfrac{q\varepsilon_s N_d}{2(\phi_i - V)}} & W < W_i \\ C_j = A_j\varepsilon_s / W_i & W \geq W_i \end{cases} \tag{2}$$

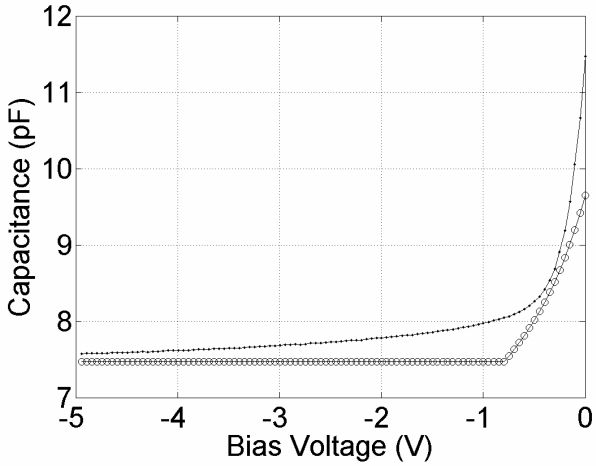

Fig. 7. Total capacitance measured from demonstrated photodiode element at 1MHz under room temperature with dotted line. The "o" line is the calculated capacitance of PN junction and contact pad at room temperature with assumption and certain material parameters.

C. *Light responsivity*

Light responsivity, also called light sensitivity, is defined in (3) according to [5], where η is the quantum efficiency, λ is the wavelength of the incident light, h is the Planck's constant, c is the light speed and q is the electronic charge. In the measurement setup, a monochrometer was used to scan over a spectral range from 320nm to 1040nm of a mercury lamp source. The outcoming light was collimated to the active area of the photodiode. The light current of both specimen and a calibrated photodiode were measured from the amperometer at zero bias voltage. The power of the incoming light was calculated by using the known properties of the calibrated photodiode. In order to make the incident light safely fall into the active area of the photodiode, a 25mm^2 monitor diode with the TWI taken from the same processed wafer was used as the sample diode. In addition to the sample diode, another monitor diode with the 25mm^2 active area but without the TWI taken from the same processed wafer was also measured. The measured responsivity data can be seen in Fig. 8, where the

two curves from two monitor diodes show that the TWI has nearly no effect on the light responsivity. The straight line in Fig. 8 gives the ideal light responsivity with the quantum efficiency of 100%. The quantum efficiency is close to 80% for the demonstrated sample diodes under the wavelength from 500nm to 840nm by using (3). The quantum efficiency can be further improved by using additional antireflection layers.

$$\frac{I_{opt}}{P_{opt}} = \eta \frac{q\lambda}{hc} \tag{3}$$

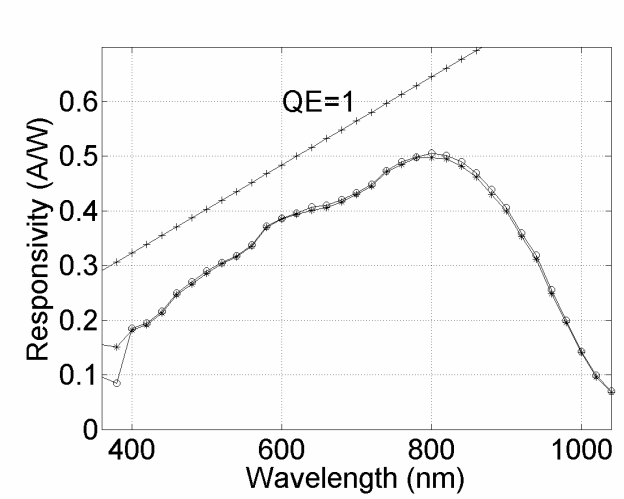

Fig. 8. Light responsivity from the sample diodes at room temperature. The "o" line is measured from sample diode with TWI, the "*" line is measured form sample diode without TWI, and most of the "o" line and "*" line is overlapped each other. The "+" line is the ideal reponsivity calculated by assuming quantum efficiency equal to 100%.

D. Rise time and fall time

The rise time of the photodiode is defined as the output signal rising from 10% to 90% of the steady state value, and fall time is defined in the opposite direction, output signal falling from 90% to 10%. The circuit of the measurement setup can be seen in Fig. 9, where I_{ph} is the photo current generated in the photodiode under testing by using a laser LED illumination driven with square waveform at low frequency, C_D is the total capacitance of the photodiode including junction capacitance, TWI capacitance and terminal capacitance, R_S is the series resistance of the photodiode including the diode resistance, TWI resistance and terminal resistance, R_f is the feedback resistance in the operational amplifier circuit and R_{sh} is the shunt resistance of the photodiode. The output can be calculated by using (4), assuming that the shunt resistance is infinite.

$$V_{out} = \frac{R_f}{1 + j2\pi f C_D R_S} I_{ph}. \tag{4}$$

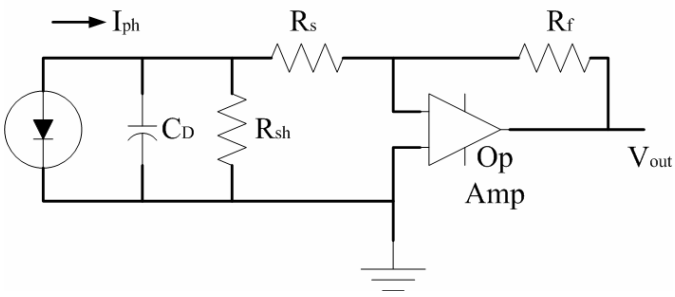

Fig. 9. Modeling of photodiode and operational amplifier circuit.

It can be seen from (4) that the total capacitance and series resistance contribute to the RC delay time, which is given by

$$t_1 = 2.2 R_S C_D. \tag{5}$$

In addition to the RC delay time, there are two additional delay time due to photo current being collected by carrier drifting within the space charge region, and by carrier diffusion within the quasi natural region. The delay time caused by drifting can be evaluated by (6), where W is the depletion width of the junction, μ_p is the drift mobility of holes in the space charge region. The delay time caused by the diffusion can be evaluated by (7), where L is the diffusion length from the quasi natural region to the edge of the space charge region and D_p is the diffusion coefficient of holes in the quasi natural region. Both drifting delay time and diffusion delay time are very small compared to the RC delay time when using the material parameters and dimensions of the demonstrated samples.

$$t_2 = \frac{W^2}{\mu_p(\phi_i - V)} \tag{6}$$

$$t_3 = \frac{L^2}{2D_p} \tag{7}$$

Therefore, the total delay time combining all three components can be given by

$$t = \sqrt{t_1^2 + t_2^2 + t_3^2} \approx t_1. \tag{8}$$

The same 25mm^2 active area samples used in light responsivity measurement were also used in the rise and fall time testing. Applying the delay time analysis above, the rise and fall times of the samples can be estimated. The photodiode sample in the package with the TWI structure has the capacitance of about 227pF and the series resistance of about 242Ω, which gives to the calculated rise and fall times of about 124ns.

Utilizing the laser LED with the dominant wavelength of about 637nm to illuminate the test diode with the TWI at 25kHz frequency, the rise and fall times of about 125ns were measured. This shows that the test result matches very well with the theoretical analysis. On the other hand, the sample photodiode without TWI has the measured rise and fall times of about 60ns. The difference between the two measured results gives the effect of the TWI resistance on the rise and fall times. In practice, functional photodiode elements in real detectors will have much shorter rise and fall times, because the PN junction area and related capacitance will be much smaller. Meanwhile, the CT systems are using the scintillation layer on top of the detector to convert the X-rays to the visible light spectra. Therefore the requirement on the rise and fall times of the detector is in the range of micro second.

IV. Conclusions

The advanced photodiode detector presented in this paper shows that it achieves a true 2D extension ability for medical imaging, especially X-ray CT application, by integrating TWI technology into the conventional front illuminated photodiode structure. The photocurrent signal can be wired out from the back side of the detector, which gives possibility of building up arbitrarily large area detectors for CT equipments. The measurement results of the demonstrated detectors and samples presented in this paper show that the performance essentially meets or exceeds the requirements of the modern CT systems.

Acknowledgment

The authors would like to thank Kimmo Henttinen and Tuula Virolainen of VTT for their contributions to the TWI processing reported in this paper. The authors would like to acknowledge Wang Yong, Zeng Ying, Mikael Kroneld and Sami Juottonen at Detection Technology Inc. for their support in photodiode design and testing. As a Ph.D student, the author would also like to thank Prof. Harri Lipsanen from Micro and Nanosciences Laboratory, Helsinki Univeristy of Technology for reviewing the paper.

References

[1] W. A. Kalender, Computed tomography, Publicis Corporate Publishing, Erlangen, 2005, pp. 58.

[2] R. Luhta, R. Mattson, N. Taneja, P. Bui, R. Vasbo, "Back Illuminated Photodiodes for Multislice CT," Medical Imaging 2003: Physics of Medical Imaging, Proceedings of the SPIE, Vol. 5030, pp. 235-245 (2003).

[3] R. Luhta, M. Chappo, B. Harwood, R. Mattson, D. Salk, C. Vrettos, "A new 2D-tiled detector for multislice CT," Medical Imaging 2006: Physics of Medical Imaging, Proceeding of SPIE, Vol. 6142, pp. 275-286 (2006).

[4] F. Ji, S. Leppävuori, I. Luusua, S. Eränen, I. Hietanen, M. Juntunen, "Fabrication of Silicon Based Through-wafer Interconnects for Advanced Chip Scale Packaging", Proceedings of Eurosensors Conference XX, Vol I, pp. 188-189 (2006).

[5] M. Fukuda, Optical semiconductor devices, John Wiley & Sons, 1999, pp. 211-219.

[6] P. Bhattacharya, Semiconductor optoelectronic devices, Prentice-Hall International, Inc., 1994, pp. 171-175.

[7] L. W. Schaper, D. I. Amey, "Improved electrical performance required for future MOS packaging," IEEE Transactions On Components, Hybrids, And Manufacturing Technology, Vol. CHMT 6, No. 3, pp. 283-289 (1983).